JOURNAL OF MATERIALS SCIENCE **39** (2004) 3647– 3657

Ultrasonic spray pyrolysis for nanoparticles synthesis

S. C. TSAI
Institute for Applied Science and Engineering Research, Academia Sinica, Taipei 115, Taiwan; Department of Chemical Engineering, California State University, Long Beach, CA 90840, USA

Y. L. SONG
Institute for Applied Science and Engineering Research, Academia Sinica, Taipei 115, Taiwan

C. S. TSAI
Institute for Applied Science and Engineering Research, Academia Sinica, Taipei 115, Taiwan; Department of Electrical and Computer Engineering, University of California, Irvine, CA 92697, USA
E-mail: cstsai@uci.edu

C. C. YANG, W. Y. CHIU
Department of Chemical Engineering, National Taiwan University, Taipei, Taiwan

H. M. LIN
Department of Material Engineering, Tatung University, Taipei, Taiwan

This article presents new findings regarding the effects of precursor drop size and precursor concentration on product particle size and morphology in ultrasonic spray pyrolysis. Large precursor drops (diameter $> 30\,\mu$m) generated by ultrasonic atomization at 120 kHz yielded particles with holes due to high solvent evaporation rate, as predicted by the conventional one particle per drop mechanism. Precursor drops 6–9 μm in diameter, generated by an ultrasonic nebulizer at 1.65 MHz and 23.5 W electric drive power, yielded uniform spherical particles 90 nm in diameter with proper control of precursor concentration and residence time. Moreover, air-assisted ultrasonic spray pyrolysis at 120 kHz and 2.3 W yielded spherical particles about 70% of which were *smaller* than those produced by the ultrasonic spray pyrolysis of the 6–9 μm precursor drops, despite much larger precursor drop size (28 μm peak diameter versus 7 μm mean diameter). These particles are much smaller than predicted by the conventional one particle per drop mechanism, suggesting that a gas-to-particle conversion mechanism may also be involved in spray pyrolysis.

1. Introduction

Spray pyrolysis is widely used in industry to produce fine-grained ($>0.5\,\mu$m diameter) powders because it is relatively inexpensive and quite versatile. Spray pyrolysis is a continuous flow process that operates at ambient pressure; therefore, it is more economical than other processes (such as sol-gel and chemical vapor deposition) that involve multiple steps or must be conducted under vacuum. Moreover, its chemical flexibility offers numerous opportunities for controlled synthesis of advanced ceramic powders and films [1]. However, the mechanisms of spray pyrolysis are at present not fully understood. Understanding of these mechanisms is essential to evaluating the potential of spray pyrolysis for the mass production of uniform nanoparticles of materials such as zirconia and titania, which are used in thermal insulation, solid oxide fuel cells [2], gas sensing [3], photo catalysis, and many other applications [3].

Spray pyrolysis involves four major steps: (1) generation of drops from a precursor solution, (2) drop size shrinkage due to evaporation, (3) conversion of precursor into oxides, and (4) solid particle formation. Drops are typically generated through either two-fluid atomization (*liquid* atomization by high velocity *air*) or ultrasonic atomization (without air) [4]. Two-fluid atomization has the advantage of high throughput but also has the disadvantage of broad drop size distribution (which results in broad particle size distribution). On the other hand, ultrasonic atomization has the disadvantage of low throughput, but has the advantage of narrow drop size distribution (and therefore, narrow particle size distribution). Furthermore, by increasing the ultrasonic frequency, one can decrease the drop size

[5, 6]. It is widely believed that the drops, when sprayed into a tubular reactor under pyrolysis conditions, serve as micro-reactors and yield one particle per drop [1].

The drop sizes obtained by different atomization techniques have been found to significantly affect the size and morphology of the particles produced [4]. However, the actual relationship between precursor drop size and the resulting product particle size has yet to be determined. This may be because previous studies either have merely estimated drop size using mathematical equations, or have produced particle size distributions that were too broad to elucidate the relationship between drop size and particle size. For example, Milosevic *et al*. [4] used ultrasonic atomization to create spherical solid $BaTiO_3$ particles with mean diameter of 0.53 μm, and used two-fluid atomization to create larger particles with mean diameter of 4 μm. Although the respective drop sizes generated by these two atomization techniques were reported to be 2.2 and 15.5 μm [4]), these numbers were estimated mathematically rather than obtained through actual measurement. Specifically, the 2.2 μm drop diameter was estimated at 2.5 MHz ultrasonic frequency using the Kelvin equation multiplied by 0.34 [7], which often underestimates the drop diameter [5, 6], and the 15.5 μm drop diameter was estimated using an empirical equation for two-fluid atomization [8]. Although Zhang and Messing [9] actually measured the drop size (mean diameter about 10 μm) in two-fluid atomization of zirconium acetate, they produced globules of zirconia (ZrO_2) particles ranging in size from 0.5 to 2 μm in diameter, many of which were irregularly shaped. Thus, the relationship between drop size and particle size was difficult to assess in this study.

Recently, we reported a new atomization technique—called ultrasound-modulated two-fluid (UMTF) atomization or air-assisted ultrasonic atomization [5, 6, 10]—that has a higher throughput and produces a narrower drop size distribution and a smaller peak drop diameter (the diameter where the peak of a drop-size distribution occurs) than conventional ultrasonic atomization (without air) at the same ultrasonic frequency [5]. For example, while conventional ultrasonic atomization yields a bimodal drop-size distribution (a primary peak at 55 μm and a much weaker secondary peak at 22 μm diameter) at 110 kHz, addition of air at 170 m/s velocity and 5.6 mA/mL (ratio of air- to liquid-mass flow rate) in UMTF atomization yields water sprays with a single peak at 22 μm drop diameter generated by the third harmonic frequency of 330 kHz [5]. Because UMTF atomization produces more uniform drop size, heat and mass transfer rates are easier to manipulate, resulting in greater control over particle size during spray pyrolysis. By comparing UMTF atomization with conventional ultrasonic atomization techniques (with both commercial ultrasonic nozzles and home-made ultrasonic nebulizers) and by varying drop size (with peak diameters ranging from 7 to 55 μm), the present study examined quantitatively the relationship between precursor drop size and resulting particle size in spray pyrolysis. We found that the particles produced by UMTF spray pyrolysis are much smaller than those produced by conventional ultrasonic spray pyrolysis. A careful comparison of precursor drop sizes to product particle sizes reveals that in addition to the conventionally-accepted one particle per drop mechanism [1], spray pyrolysis may also involve the gas-to-particle conversion mechanism, which creates nanoparticles much smaller than those predicted by the one particle per drop mechanism alone.

2. Experimental setup

2.1. Spray pyrolysis system

A schematic diagram of the bench-scale spray pyrolysis system used in this study is shown in Fig. 1. Major components of the system are: (1) a three-zone furnace 130 cm in length (Linberg Model Blue M), (2) 3″- and 1″-tubular quartz reactors (7.6 and 2.5 cm ID

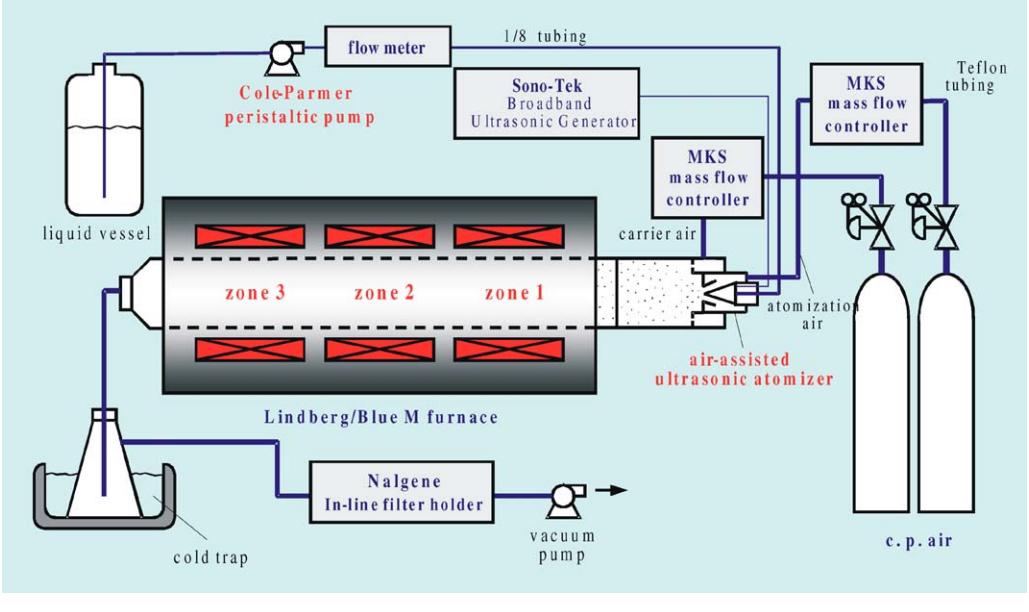

Figure 1 Schematic diagram of spray pyrolysis system.

and 170 cm length) located in the furnace, (3) an atomizer for generation of sprays (precursor drops), and (4) precision flow meters and controllers (MKS Model 1179, Andover, MA). As shown in this figure, carrier air is supplied upstream and a vacuum pump is provided downstream from the reactor for control of the residence time of the precursor drops flowing through the reactor. The resulting product particles are collected in liquid nitrogen cold traps and on a filter positioned between the traps and the vacuum pump. The 3″-tubular reactor was used unless specified otherwise.

The operating temperatures of the furnace varied from 200 to 1100°C, with accuracy of ±3°C. The temperature of zone 2 of the furnace was set at 650, 700, and 750°C while the temperatures of zone 1 and zone 3 were set at 200 and 350°C, respectively. The rates of airflow through the reactor ranged from 20 to 31 L/min. The water flow rate was 5 cc/min when either a Sono-Tek 120 kHz ultrasonic nozzle or an UMTF atomizer was used, but was less than 0.3 cc/min when a 1.65 MHz ultrasonic nebulizer was used. The temperatures at several points along the axis of the reactor were measured using a Type K (NiCr-NiAl) thermocouple with accuracy of ±2.5°C. These temperatures, independent of the air and water flow rates, are shown in Fig. 2. Based on the temperature profiles in Fig. 2, the flow rates of carrier air along the axis of the reactor were first calculated for three different flow rates (20, 25, and 31 L/min at standard conditions) assuming ideal gas. Division of the flow rates by the cross sectional area of the tubular reactor gave rise to the carrier air velocities along the reactor axis, yielding the temperature-residence time profiles in Fig. 3 for air-entrained drops or particles near the axis in both 3″ (7.5 cm)- and 1″ (2.5 cm)-tubular reactors. This figure shows that the residence time at the same maximum reactor temperature and carrier airflow rate is reduced by an order of magnitude as the tube diameter is reduced from 7.5 to 2.5 cm.

An UMTF atomizer consists of an annulus for airflow and an ultrasonic nozzle (Sono-Tek Model 8700-120, Milton, NY) with a central channel (0.93 ± 0.02 mm

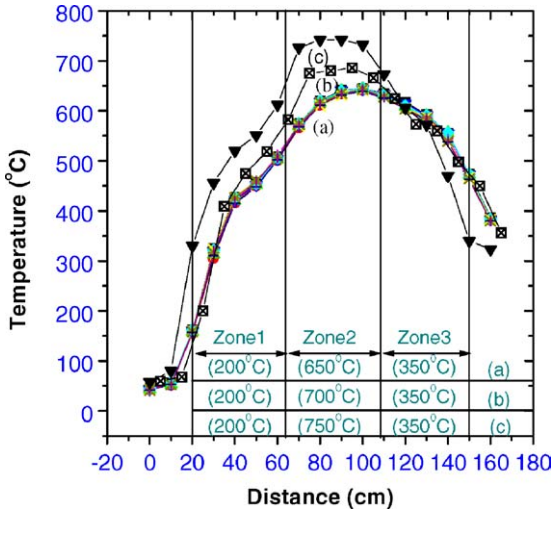

Figure 2 Temperature profile of the three-zone tubular reactor of the spray pyrolysis system at maximum set point temperatures of (a) 650°C, (b) 700°C, and (c) 750°C.

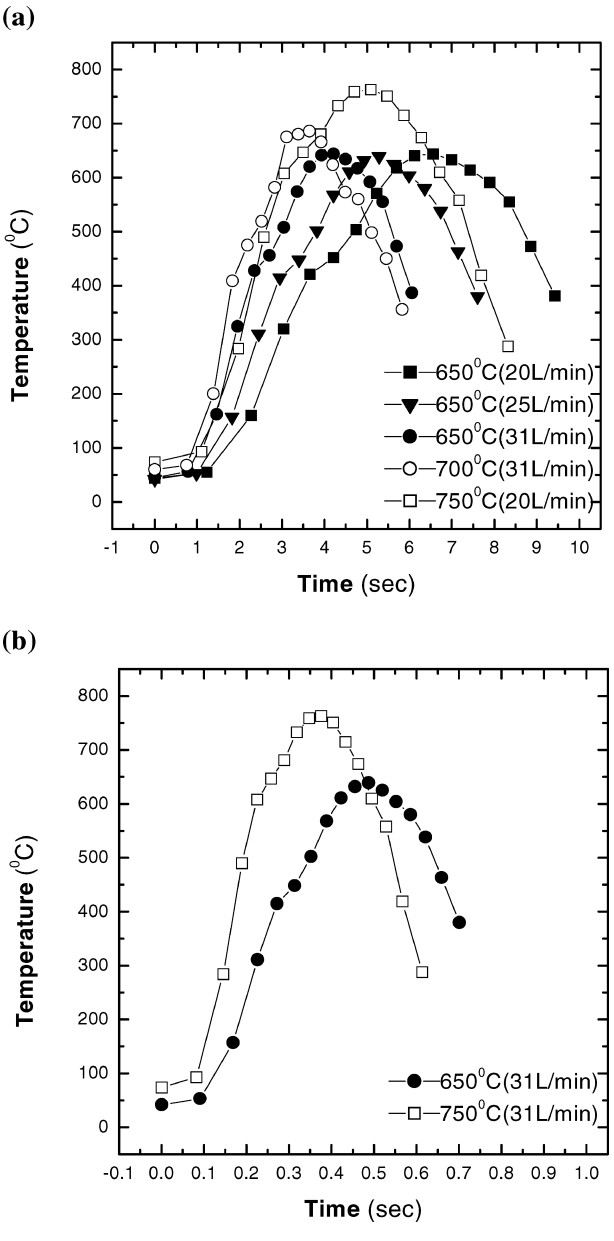

Figure 3 Temperature-Residence time profiles at airflow rates of 20, 25, and 31 L/min for quartz tubular reactors (a) 3″ or 7.5 cm and (b) 1″ or 2.5 cm in diameter.

diameter) for liquid flow [10]. The Sono-Tek ultrasonic nozzle consists of a pair of washer-shaped ceramic (PZT) piezoelectric transducers and a titanium resonator. The transducers, surrounding the central channel, are sandwiched in the titanium resonator located in the large diameter (about 3.6 cm) portion of the nozzle body. The piezoelectric transducers receive an electrical input at the nozzle resonant frequency from a broadband ultrasonic generator (Sono-Tek Model 06-05108), and convert the input electrical energy into mechanical energy of vibration. The nozzle is a half wavelength design with a resonant frequency (f) of 120 kHz. It is geometrically configured such that excitation of the piezoelectric transducers creates a standing wave through the nozzle, with the maximum vibration amplitude occurring at the nozzle tip. The outside diameter of the nozzle tip and the length of the front horn measure 3.12 mm and 1.4 cm, respectively. As a liquid jet issues from the nozzle tip, a liquid capillary wave is initiated

by the ultrasound. The capillary wave travels axially along the jet in the direction of the liquid flow, and its amplitude grows exponentially due to amplification by the air blowing around it. Atomization occurs when the amplitude becomes too great to maintain wave stability.

The homemade ultrasonic nebulizer used in this study consists of a PZT disk transducer 1.6 cm in diameter with a resonant frequency (f) of 1.65 MHz (King Ultrasonics Co., Ltd., Taipei, Taiwan). Liquid is continuously fed to the reservoir to maintain a constant liquid level (about 3 cm) above the PZT transducer; an adjustable cap is provided to prevent entrainment of large drops by the carrier air. The transducer is driven by a sine wave generated by a function generator (Agilent Technologies Model 33120A, Palo Alto, CA, USA) after amplification (Amplifier Research Model 75A250, Souderton, PA, USA). A 50 dB dual directional coupler (Model DC2600, Amplifier Research) is used to divert 10^{-5} of the amplified signal to an oscilloscope (Agilent Technologies Model 54621A) for frequency tuning, waveform confirmation, and power measurement. A drive power of 23.5 $\pm$ 0.5 W (actual input power to the transducer, which equals the total power subtracted by the power loss due to impedance mismatch), was required to maintain stable atomization.

2.2. Drop size analysis system

A schematic diagram of a drop size analysis system similar to the one used in this study has been presented elsewhere [5]. The main part of the system is an ensemble laser diffraction instrument (Malvern Spraytec RTS 5000). This instrument uses a solid-state laser light at 670 nm wavelength to illuminate the drops and Fraunhoffer diffraction theory to calculate drop size from the resulting scattered light. The scattered light is collected from the forward direction by a log-scaled annular detector lens that is composed of discrete elements. Because large drops scatter light at small forward angles, and small drops scatter at large forward angles, the scattered light intensities collected by the discrete annular elements of the detector lens give rise to drop sizes and drop size distributions that are presented as frequency plots of volume percentage versus drop diameter on a semi-logarithmic scale. The instrument was calibrated using a reticle (Malvern/INSITEC Model #RS-3).

3. Experimental results

Characterizations of the precursor used and the conversion products are first presented followed by a description of the precursor drop size and size distributions used in this study. As the precursor drops (entrained in the carrier air stream) flow through the tubular reactor at a fixed temperature profile (see Fig. 2), the temperature-residence time changes as a function of carrier airflow rates of 20, 25, and 31 L/min (standard conditions) as shown in Fig. 3. Also indicated in this figure are the heating rates of the drops at these carrier airflow rates. How particle size and morphology vary with drop size and precursor concentration will be presented in this section.

3.1. Characterizations of precursor and products

The precursor used in this study was zirconium hydroxyl acetate (ZHA), reagent grade from Aldrich Chemical (Milwaukee, WI). Its chemical formula was $Zr(OH)_x(CH_3COO)_{4-x}$, where $x = 2.64$ and the molecular weight was 216 with the weight fraction of ZrO_2 being 0.57. The precursor was characterized by thermal gravitational analysis (TGA) and Differential Scanning Calorimetry (DSC) analysis; the results are shown in Fig. 4a and b. TGA was carried out in a Perkin-Elmer Model TGA-7 under gaseous nitrogen flow for removal of product gases. DSC was carried out in a closed system (Dupont Model 2010). The difference between the sample and reference cells in the heat required to reach a given temperature at a specified heating rate was recorded. Note that the 2nd run in Fig. 4b uses the same sample as the 1st run (without the volatiles that were removed in the 1st run). The TGA curves in Fig. 4a show

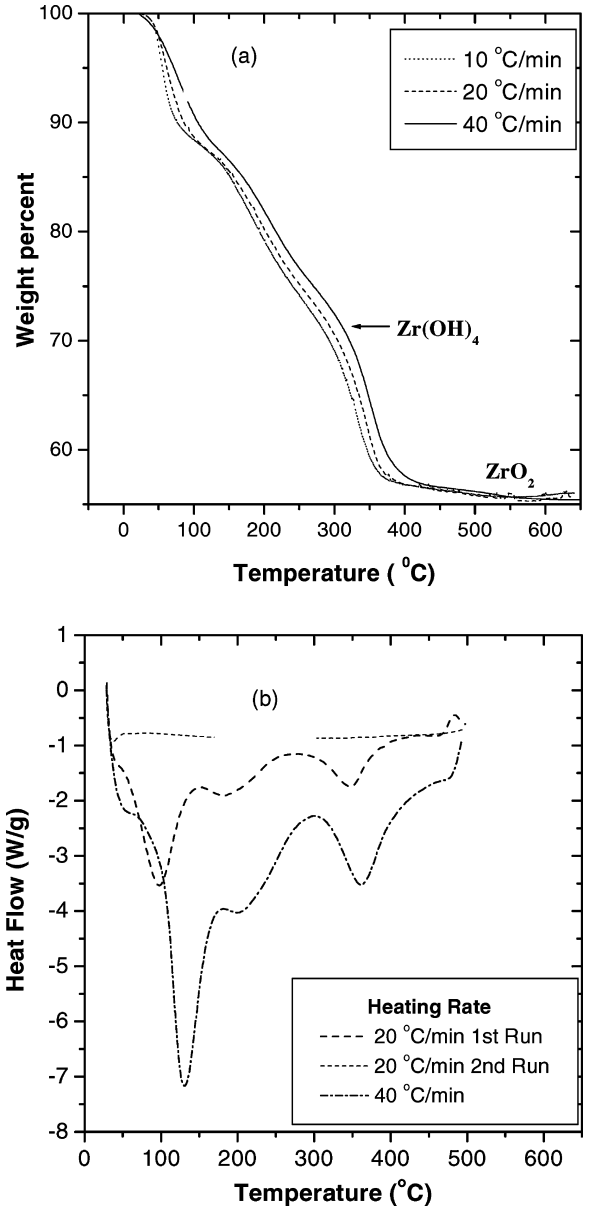

Figure 4 (a) Thermal gravitational analysis (TGA) and (b) Differential Scanning Calorimetric (DSC) Analysis of precursor zirconium hydroxyl acetate (ZHA).

a slightly lower residual weight fraction (0.55 versus 0.57) than the molecular weight ratio of ZrO_2 to ZHA as a result of water adsorption of approximately 4%. Fig. 4a shows 10% water loss and, thus, indicates that the $Zr(OH)_x$ group in ZHA used may exist partially as zirconyl oxide hydrate $ZrO\text{-}H_2O$. Using 96% as a weight correction factor, complete conversion of ZHA to $Zr(OH)_4$ should yield residual weight of 71% as indicated in the figure.

Based on Fig. 4a, four different weight loss mechanisms take place in temperature ranges of 50–150°C, 150–300°C, 300–400°C, and 400–600°C. The weight loss in temperature ranges 50–150 and 400–600°C can be attributed to water evaporation and conversion into ZrO_2. Weight loss in the two middle temperature ranges may be attributed to decomposition of ZHA to acetic acid and $Zr(OH)_4$, and subsequent evaporation of the products. This interpretation is born out by the DSC curves in Fig. 4b. This figure shows the heat absorption reaction at 100°C due to water evaporation and the exothermic reaction near 500°C due to conversion into ZrO_2. It also shows two heat absorption peaks at 175 and 350°C. The 175°C peak can be attributed to evaporation of acetic acid (normal boiling point in pure state 120°C) which was collected and identified. The 350°C peak may be attributed to evaporation of zirconium hydroxide (amorphous white powder).

Precursor solutions were prepared by dissolving Yttria-containing ZHA (3 mol% Y_2O_3 and 97 mol% ZrO_2) in de-ionized water [11]. A precursor concentration of 5 wt% was used unless specified otherwise. The surface tension and the kinematic viscosity (ν) of the precursor solution were measured using a Kruss Digital-Tensiometer K9 and a Cannon-Fenske viscometer, respectively. They were found to resemble those of de-ionized water.

Fig. 5a–c shows the X-ray Diffraction (XRD) patterns measured by a Model MXP-18, MacScience Co. (Japan) for the particles produced by spray pyrolysis at 650, 700, and 750°C, respectively. The XRD signals at 700 and 750°C were identified as yttria stabilized zirconia (YSZ), tetragonal phase. The XRD signals at 650°C were less sharp (and therefore, less clearly identified as YSZ); however, after annealing these particles at 800°C for 30 min, the XRD signals were as sharp as those at 750°C, and thus, were also identified as YSZ.

The size and morphology of the product particles were characterized using Scanning Electron Microscopy (SEM, Hitachi Model S-4200, Japan). 10 to 20 SEM micrographs were obtained for each spray pyrolysis experiment from which two to four representative graphs were selected for counting of particles to determine their size distribution and mean diameter. Note that the number of particles counted to obtain a particle size distribution falls in the range of 450 to 1500, more typically 800. The accuracy of the (number) mean diameter was found to be ±4% or better.

3.2. Drop size and size distributions of precursor solutions

Fig. 6 shows the drop sizes and size distributions obtained in both ultrasonic atomization and UMTF atomization of precursor solutions at conditions used in spray pyrolysis. In this figure, mass median diameter (MMD) designates the drop diameter at 50% of the cumulative drop size distribution; volume mean diameter (VMD) and Sauter mean diameter (SMD) are the mean diameters based on the volume and the surface, respectively. Fig. 6 shows that the drops from UMTF atomization (at ultrasonic power of 2.3 W, air velocity of 150 m/s, and ratio of air-to-liquid mass flow rate mA/mL of 4.1) were much smaller and more uniform in size than those from conventional ultrasonic atomization at the same ultrasonic frequency (120 kHz). Specifically, the MMD and VMD for the UMTF atomized drops were 37 and 44 μm, respectively. The corresponding values for the conventional ultrasonic atomization were 59 and 68 μm. The half width of the drop-size distribution was 40 μm for

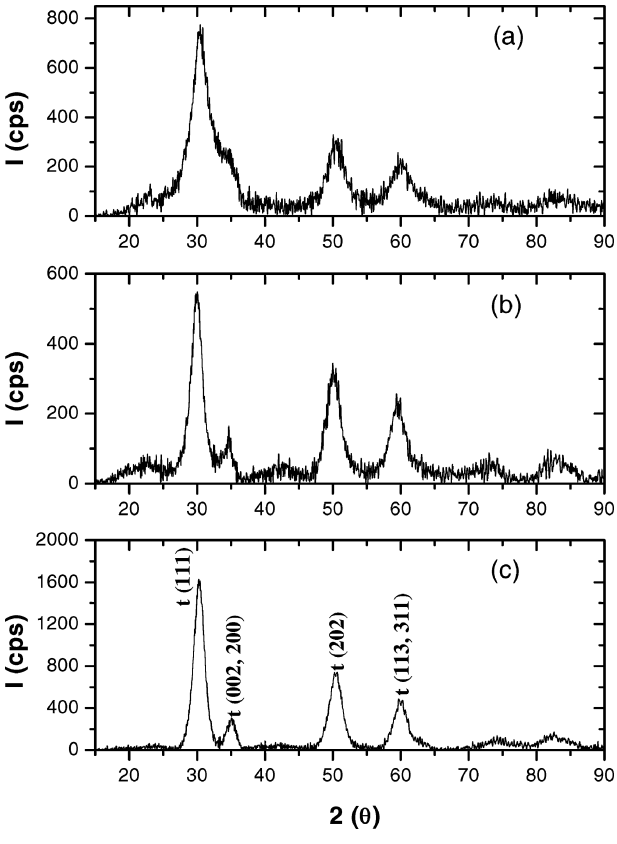

Figure 5 XRD patterns of product particles as received from spray pyrolysis at (a) 650°C, (b) 700°C, and (c) 750°C.

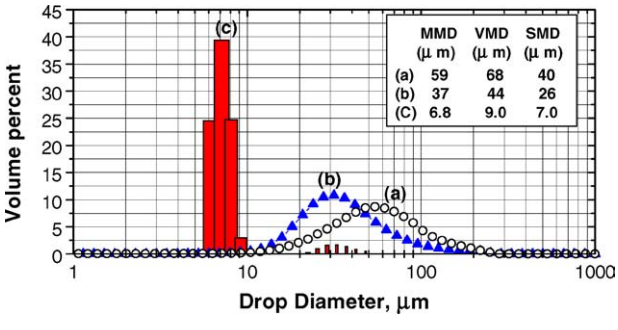

Figure 6 Drop size distributions for (a) ultrasonic atomization using a Sono-Tek nozzle at 120 kHz and 2.3 W, (b) UMTF atomization at 120 kHz, 2.3 W, 150 m/s air, and 4.1 mA/mL, and (c) ultrasonic atomization using a home made nebulizer at 1.65 MHz and 24 W.

UMTF atomization, and 70 μm for conventional ultrasonic atomization. The respective peak diameters were 28 and 55 μm. Also shown in Fig. 6 are the 6–9 μm drops generated by the homemade nebulizer with the PZT disk transducer at 1.65 MHz and 23 W, which were much more uniform, with MMD of 6.8 μm and VMD of 9 μm.

3.3. Effects of precursor drop size and size distribution

Fig. 7a shows the SEM micrograph of the powders (yttria stabilized zirconia, YSZ) obtained by spray pyrolysis at 650°C of precursor drops with the drop size distribution shown in Fig. 6, curve (a), generated by conventional ultrasonic atomization at 120 kHz and 2.3 W. The flow rates of the carrier air and the precursor solution used in the spray pyrolysis experiment were 25 L/min and 5 cc/min, respectively. Likewise, Fig. 7b shows the SEM micrograph from spray pyrolysis of precursor drops with the drop size distribution shown in Fig. 6, curve (c) obtained using the 1.65 MHz nebulizer. The spray pyrolysis temperature was also 650°C, but the carrier airflow rate was slightly lower (20 versus 25 L/min) and the liquid flow rate was less than 0.3 cc/min. As shown in Fig. 3, the slower airflow rate also led to slower heating time. Clearly, the resulting YSZ particles in Fig. 7b are much smaller and more uniform than those in Fig. 7a. These results were consistent with the much smaller and more uniform precursor drops (6-9 μm) generated by the 1.65 MHz nebulizer (see Fig. 6). More importantly, while the large YSZ particles in Fig. 7a generated from the large drops with 59 μm MMD have holes, the much smaller YSZ particles in Fig. 7b generated from the 6–9 μm drops are spherical and free from holes.

Fig. 7c shows the SEM micrograph of the YSZ particles obtained in spray pyrolysis of precursor drops with the drop size distribution given in Fig. 6, curve (b) generated by UMTF atomization (120 kHz, 2.3 W, 150 m/s air velocity, and 4.1 mA/mL). The maximum temperature of spray pyrolysis was 650°C; the flow rates of the 5 wt% precursor solution and the carrier air were 5 cc/min and 31 L/min, respectively. A comparison of Fig. 7c to a, on two different scales, reveals that the YSZ particles generated by UMTF spray pyrolysis were much smaller than those generated by conventional ultrasonic spray pyrolysis at the same ultrasonic frequency (120 kHz). These results were consistent with the much smaller drop size achieved by UMTF atomization than by the conventional ultrasonic atomization as shown in Fig. 6, curve (b) versus curve (a).

A comparison of Fig. 7c and b shows that, as expected, the particles generated by UMTF spray pyrolysis at 120 kHz were less uniform than those generated by the conventional ultrasonic nebulizer operating at a much higher frequency (1.65 MHz) and much higher electric drive power (23.5 W versus 2.3 W). Careful counts of 1126 and 908 particles from the SEM micrographs as represented by Fig. 7c and b yielded the particle size distributions shown in Fig. 8a and b, respectively. Fig. 8a shows that as many as 97% of the YSZ particles generated by UMTF spray pyrolysis were smaller than the 1 μm diameter predicted by the conventional one particle per drop mechanism for 5.0 wt% precursor concentration (see Table I). Furthermore, a comparison of Fig. 8a and b clearly shows that not only was the mean particle diameter smaller (0.39 versus 0.65 μm) for UMTF spray pyrolysis than for ultrasonic

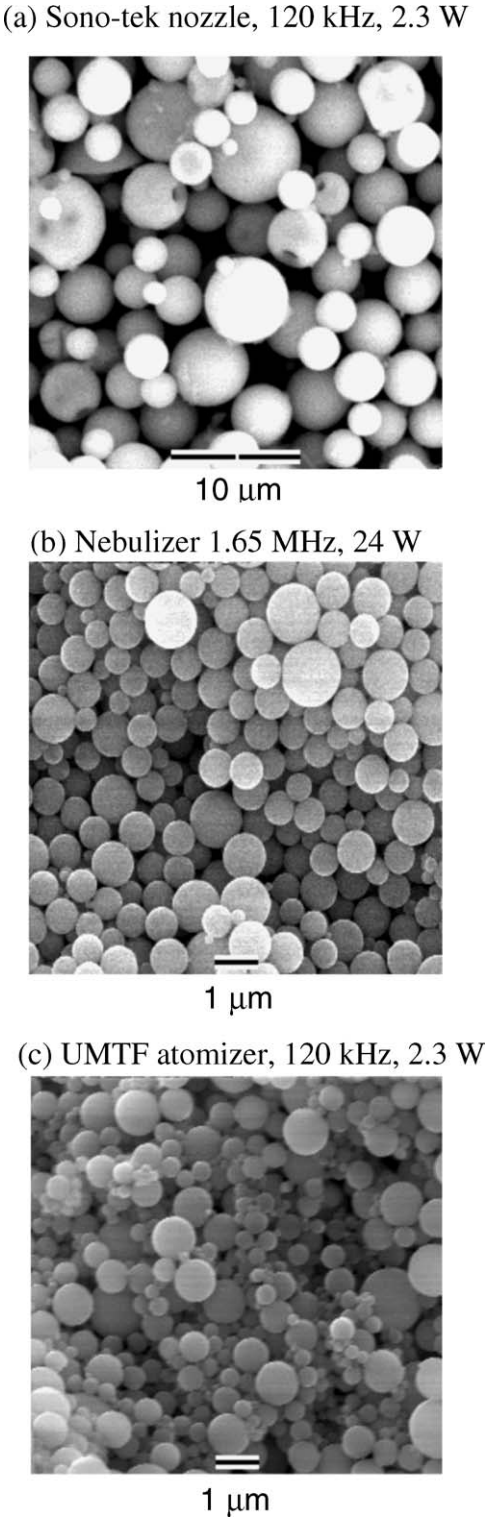

Figure 7 SEM micrographs of particles from spray pyrolysis at 650°C (with respective carrier airflow rates of 25, 20, and 31 L/min) using a 3″-tubular reactor for 5 wt% precursor drops generated by (a) conventional ultrasonic atomization at 120 kHz, (b) ultrasonic nebulizer atomization at 1.65 MHz, and (c) UMTF atomization at 120 kHz, 2.3 W, 150 m/s air velocity, and 4.1 mA/mL.

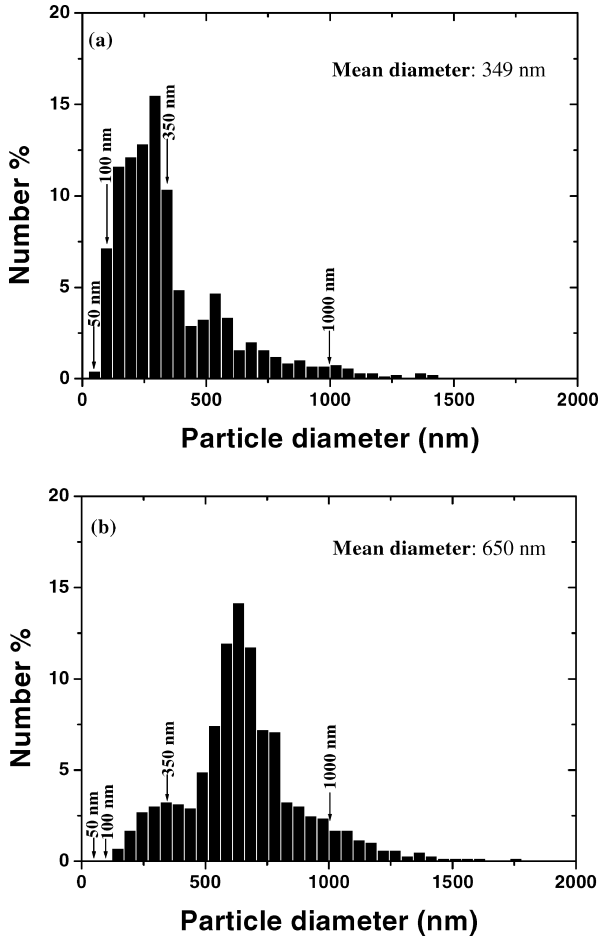

Figure 8 Particle size distributions from spray pyrolysis at 650°C (respective liquid flow rates of 5 and <0.3 cc/min, and carrier airflow rates of 20 and 31 L/min) using a 3″-tubular reactor and 5 wt% precursor drops generated by (a) UMTF atomization at 120 kHz, 2.3 W, 150 m/s air velocity, and 4.1 mA/mL, and (b) ultrasonic nebulizer atomization at 1.65 MHz.

nebulizer pyrolysis, but also 70% of the YSZ particles generated by UMTF spray pyrolysis were smaller in diameter than the 0.35 μm predicted based on the conventional one particle per drop mechanism for precursor drops 6 μm in diameter at 0.2 wt% (Table I), compared to 11% for the ultrasonic nebulizer. These findings were very surprising in view of the much larger precursor drop size generated by the UMTF atomizer compared to the ultrasonic nebulizer (peak diameter 28 versus mean diameter 7 μm) as shown in Fig. 6, curve (b) versus (c).

TABLE I Theoretical diameters (in μm) of dense spherical zirconia particles (based on the conventional one particle per drop mechanism of spray pyrolysis)

Precursor drop diameter (μm)	Zirconium-hydroxyl-acetate (precursor) concentration (wt%)		
	0.2	1.0	5.0
6	0.35	0.6	1.0
7	0.4	0.7	1.2
9	0.51	0.9	1.5
28	1.59	2.8	4.7
50	2.84	5.0	8.3

3.4. Effects of precursor concentration

The 6–9 μm precursor drops at concentrations of 1.0 and 0.2 wt% were also subjected to spray pyrolysis at 650°C using the 3″-tubular reactor and a carrier airflow rate of 20 L/min. The SEM micrographs of the resulting product particles are given in Fig. 9. A comparison of Fig. 9 to Fig. 7b clearly shows that the size of the uniform particles decreased as the precursor concentration was reduced. The measured (number) mean particle diameters were 0.65, 0.3, and 0.2 μm for precursor concentrations of 5.0, 1.0, and 0.2 wt%, respectively. Fig. 9 also shows that the particle size distribution narrowed very significantly as the precursor concentration decreased from 1.0 to 0.2 wt%. Note that the number of particles counted to obtain these size distributions exceeded 450 in Fig. 9a and 1000 in Fig. 9b. Also shown in the figures are the smallest particle diameters predicted by the one particle per drop mechanism [1]. The percentage of particles smaller than the sizes predicted by the one particle per drop mechanism (also shown in Table I) remained as high as $95 \pm 4\%$ for all three precursor concentrations.

Similar phenomena were observed for spray pyrolysis of 6–9 μm precursor drops using the 1″-tubular reactor. The maximum reactor temperature was increased to 750°C to compensate for the substantially reduced residence time mentioned previously. For example, the residence time at 600°C at the studied carrier airflow rate of 31 L/min was 0.26 s compared to 2.23 s for the 3″-tubular reactor at a carrier airflow rate of 20 L/min (see Fig. 3). As shown in Fig. 10, the mean particle diameter declined from 150 to 90 nm and the particle size distribution significantly narrowed as the precursor concentration decreased from 0.05 to 0.01 wt%. The number of particles counted to obtain the particle size distributions in these cases exceeded 860. Fig. 10 also shows that the percentage of particles smaller than the sizes (210 and 130 nm in diameter) predicted by the one particle per drop mechanism was as high as $92 \pm 2\%$.

Thus, more than 90% of the particles obtained in spray pyrolysis of 6–9 μm precursor drops were smaller than those predicted by the conventional one particle per drop mechanism. In addition, a careful examination (under SEM) of the products obtained by spray pyrolysis at the maximum reactor temperatures of 650 and 700°C using the 1″-tubular reactor at a carrier airflow rate of 31 L/min (thus, short residence time) revealed the presence of particles smaller than 50 nm in diameter as shown in Fig. 11. These experimental results clearly suggest that another mechanism may be at work.

4. Discussion

In this study, precise measurement of precursor drop size enabled us to characterize quantitatively its relationship to product particle size. By analyzing the drop-particle size relationship, we were also able to re-examine the particle formation mechanisms involved in spray pyrolysis. According to the one particle per drop mechanism [1], a viscous layer of precursor solution forms on the surface of the drop during solvent

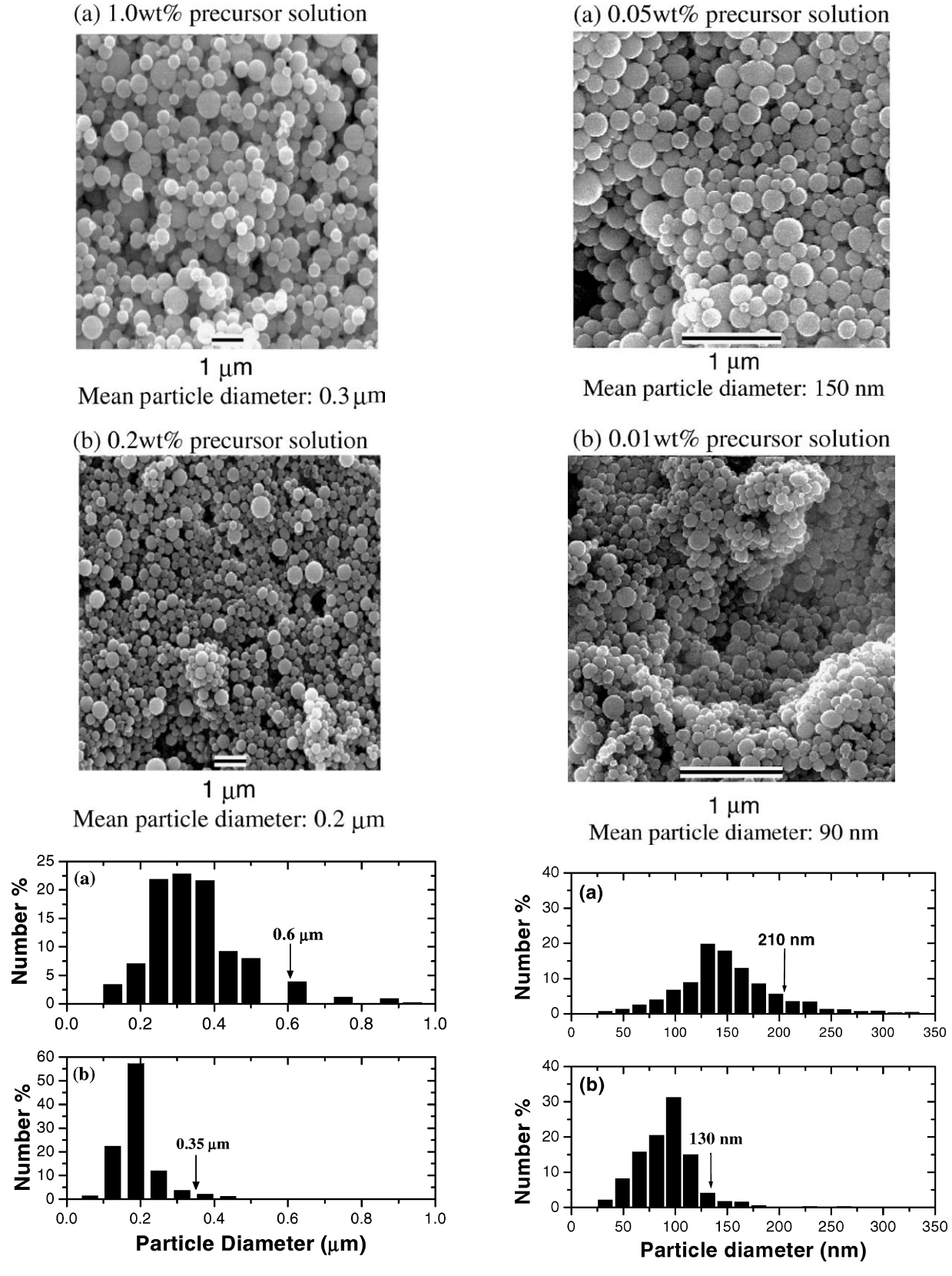

Figure 9 SEM micrographs and size distributions of particles from spray pyrolysis at 650°C and carrier airflow rate of 20 L/min using a 3″-tubular reactor for precursor drops generated by ultrasonic nebulizer atomization at 1.65 MHz and 24 W with precursor concentrations of (a) 1.0 wt% and (b) 0.2 wt%.

Figure 10 SEM micrographs and size distributions of particles from spray pyrolysis at 750°C and carrier airflow rate of 31 L/min using a 1″-tubular reactor for precursor drops generated by ultrasonic nebulizer atomization at 1.65 MHz and 24 W with precursor concentrations of (a) 0.05 wt% and (b) 0.01 wt%.

evaporation; the layer bursts at increased internal pressure, resulting in holes. However, in the current study, such holes were seen only in larger particles. Additionally, in spray pyrolysis of drops smaller than 10 μm, more than 90% of the particles were found to be smaller than predicted by the one particle per drop mechanism. Formation of holes in large particles is correlated to water evaporation rate and possible particle formation mechanisms are examined quantitatively in this section.

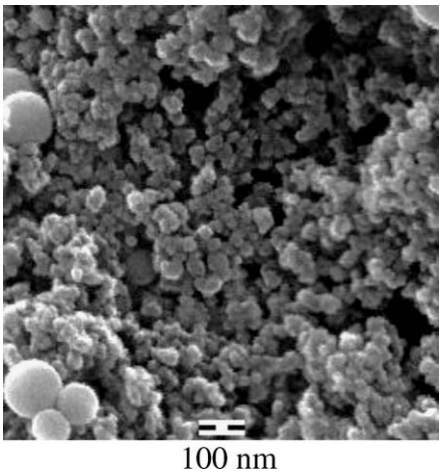

Figure 11 SEM micrograph of particles from spray pyrolysis at 650°C and carrier airflow rate of 31 L/min using a 1″-tubular reactor for 0.01 wt% precursor drops generated by ultrasonic nebulizer atomization at 1.65 MHz and 24 W.

4.1. Prediction of water evaporation rates of precursor drops

As the precursor drop goes through a temperature-residence time profile, as shown in Fig. 3, the water evaporates and the precursor solution thickens, resulting in viscous-shell formation on the surface of the precursor drop. The shell bursts when the internal pressure, due to evaporation of water, exceeds the surface tension, creating holes in the product particles. It should be noted that at saturation point (6.5 M, equivalent to 47.8 wt% ZrO_2 or 58.5 wt% $Zr(OH)_4$ or 82.4 wt% ZHA), the viscosity of the precursor solution is as high as 4.4 P [9]. The water evaporation rate is estimated as follows.

The precursor drop is approximated as a water drop because the precursor concentration used in this study was 5 wt% or less. In addition, since the liquid side heat transfer coefficient is two orders of magnitude greater than the airside of the drop, only the latter is considered. Conservation of energy leads to the following equation:

$$\lambda \times W = \pi \times d_{\text{ave}}^2 \times h \times \int_{t(100^\circ\text{C})}^{t(\text{sat'd})} [T - 100]\,\text{dt} \quad (1)$$

where λ, W, d_{ave}, h, and T are latent heat of water (2256.9 kJ/kg), weight of water evaporated during the time (t) interval from 100°C to precursor saturation temperature, average drop diameter, air-side heat transfer coefficient (taken to be 300 W/m^2-°C for saturated steam), and temperature in °C, respectively. The upper limit of integration is either the time it takes the precursor solution to reach saturation or the time it takes the drop to be completely dehydrated. d_{ave} is taken to be the arithmetic mean of the initial drop diameter and the final drop diameter. The density of the precursor solution in the calculation of the final drop diameter is taken to be 1.51 g/cc for saturated ZHA [9].

The weight of water evaporated is first calculated from the water balance for two cases: (1) when the precursor drop reaches saturation, and (2) when the drop is completely dehydrated. The time required for water evaporation in these two cases is then calculated based on Equation (1) and the heating rates for the carrier airflow rates of 20, 25, and 31 L/min given in Fig. 3 at the maximum reaction temperature of 650°C. The results are given in Table II. From the time required to reach saturation and the heating rate, one can estimate the temperature of the drop at saturation point, which is also given in Table II. This table shows that the water evaporation rates for drops of diameter smaller than 9 μm at all carrier airflow rates are very low ($<1.56 \times 10^{-6}$ cc/sec), but increase by as much as two orders of magnitude as the drop diameter increases to 50 μm. Because the Laplace equation of capillarity stipulates that the pressure difference across the film of a drop is proportional to the surface tension divided by the drop diameter, and the internal pressure of the drop is inversely proportional to the drop diameter squared, the water evaporation rate is scaled to the drop diameter, as shown in Fig. 12. This figure shows an order of magnitude increase as the drop diameter increases from 7 to 50 μm. Therefore, we believe that the high water evaporation rate accounts for the holes in the 2.5–8.5 μm-diameter particles observed in Fig. 7a for spray pyrolysis (at 650°C and 25 L/min carrier airflow rate) of the large drops (peak diameter 55 μm) generated by conventional ultrasonic atomization at 120 kHz. As expected due to the low water evaporation rate, holes are not seen in the YSZ particles produced by spray pyrolysis of the 6–9 μm drops (see Figs 7b, 9, and 10).

TABLE II Effects of drop sizes and heating rates on water evaporation rates

Drop diameter (μm)	Time (sat'd) (sec)	Time (dried) (sec)	T (sat'd) (°C)	Evap.rate (sat'd) (cc/sec)	Evap.rate (dried) (cc/sec)
Carrier airflow rate of 20 L/min at standard conditions					
6	2.06	3.5	133	5.23E-07	1.35E-09
7	2.10	3.5	136	7.57E-07	2.21E-09
9	2.16	3.5	143	1.39E-06	4.98E-09
25	2.54	3.5	209	1.58E-05	1.63E-07
50	2.94	3.5	288	1.02E-04	2.41E-06
Carrier airflow rate of 25 L/min at standard conditions					
6	1.76	2.8	140	5.24E-07	1.89E-09
7	1.80	2.8	144	7.64E-07	3.13E-09
9	1.86	2.8	153	1.42E-06	7.19E-09
25	2.21	2.8	240	1.87E-05	2.75E-07
50	2.58	2.8	239	1.10E-04	6.41E-06
Carrier airflow rate of 31 L/min at standard conditions					
6	1.44	2.2	143	5.67E-07	2.58E-09
7	1.47	2.2	147	8.30E-07	4.30E-09
9	1.52	2.2	160	1.56E-06	1.01E-08
25	1.84	2.2	268	2.11E-05	4.55E-07
50	2.16	2.2	367	1.23E-04	3.54E-05

4.2. Possible particle formation mechanisms

One particle per drop mechanism [1] is well accepted for spray pyrolysis of precursor salts with low vapor pressure. In this mechanism, each precursor drop serves as a micro reactor whose temperature varies as it travels along the three-zone tubular reactor. As the water evaporates, the diameter of the precursor drop decreases, and the precursor concentration increases. Eventually,

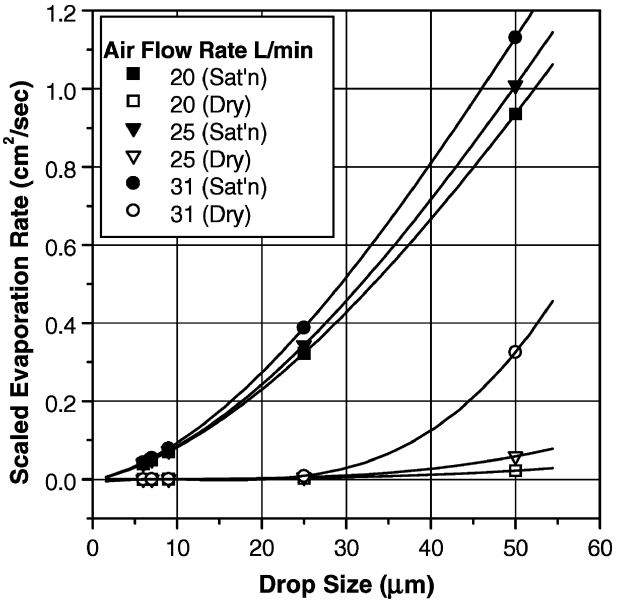

Figure 12 Calculated effects of drop size and heating rate on water evaporation rate, scaled to the drop diameter.

the precursor drop is completely dehydrated, and the precursor is converted into oxides, resulting in a dense spherical particle. Conservation of ZrO_2 mass leads to the following equation for calculation of the particle diameter (d_p) from the precursor drop diameter (d):

$$d_p = d\sqrt[3]{\frac{\rho_s w}{\rho_p}} \tag{2}$$

where w is the precursor concentration in terms of weight fraction of ZrO_2; ρ_s and ρ_p are the densities of the precursor solution (1 g/cc) and zirconia (6 g/cc), respectively. Such particle diameters for precursor drop diameters ranging from 6 to 50 μm and precursor concentrations of 0.2, 1.0, and 5.0 wt% ZHA are given in Table I. As mentioned previously, only 5 to 10% of the particles obtained in spray pyrolysis of 6–9 μm precursor drops were of the sizes predicted by this mechanism.

Gas-to-particle conversion is a well-known mechanism in combustion flame spray pyrolysis [13] and combustion flame chemical vapor condensation [14], both of which operate at temperatures above 1000°C. It is also an established mechanism in aerosol pyrolysis of metal alkoxides [15–17] that have high vapor pressure. Unlike the conventional one particle per drop mechanism, the gas-to-particle conversion mechanism involves nucleation and particle growth from gas-phase molecules, and yields particles with diameters smaller than 100 nm [18]. The presence of smaller than 50 nm-diameter particles as shown in Fig. 11 for spray pyrolysis of 6–9 μm precursor drops led us to believe that the gas-to-particle conversion mechanism must have been active. This belief is further elucidated as follows.

As the precursor drops less than 10 μm in diameter pass through the reactor, water evaporates at 100°C in less than 3 ms [12], resulting in particles of ZHA or $Zr(OH)_4$ (due to thermo-hydrolysis) with diameters much smaller than 3 μm because the precursor molecules are too far apart (see Table I for 5 wt% precursor concentration, 1.5 μm multiplied by 2, the density ratio of zirconia to precursor). The vapor pressure required for 3 μm-diameter particles at 350°C with a characteristic time (the time required to reduce the particle size by half) of 0.1 s is very small (estimated to be 0.4 torr based on the diffusion model in continuum regime, Equation 4.9, [12]). In addition, due to the Kelvin effect, the vapor pressure over the surface of a small particle is higher than that over the flatter surface of a large particle. In other words, the molecules near the surface of a small particle have fewer nearest neighbors than they would have near a large particle. As a result, less energy is required to remove a molecule from a small particle [12]. Therefore, conversion of ZHA or $Zr(OH)_4$ into zirconia, at least partially, takes place in the gas phase. Subsequently, nucleation occurs followed by particle growth, resulting in particles much smaller than the diameters predicted by the one particle per drop mechanism. Nucleation of zirconia from the gas phase is thermodynamically favorable because of its high melting point (2370°C) [19].

As mentioned previously, 70% of the YSZ particles generated in UMTF spray pyrolysis are smaller than 0.35 μm in diameter, compared to 11% when using the ultrasonic nebulizer despite the much larger precursor drop size (peak diameter 28 μm versus mean diameter 7 μm) for UMTF atomization relative to ultrasonic nebulizer atomization. This experimental result can be attributed to the much higher nucleation density since the liquid flow rate used in the UMTF spray pyrolysis is much higher (5 versus <0.3 cc/min) and the carrier airflow rate is also higher (31 versus 20 L/min) in UMTF spray pyrolysis than when using the nebulizer.

5. Conclusions

Although the effects of precursor drop size and size distribution on particle size and morphology in spray pyrolysis have been widely reported, no prior studies have quantitatively examined the specific nature of their relationship. In this study, we precisely measured drop and particle sizes and characterized this relationship. We found that: (1) particles produced by UMTF spray pyrolysis were much smaller than those produced by conventional ultrasonic spray pyrolysis and (2) precursor drop size and precursor concentration dictate product particle size and morphology. Uniform dense nanoparticles 90 nm in diameter free from cracks or holes were produced by spray pyrolysis through the use of precursor drops 6–9 μm in diameter and low precursor concentration. Furthermore, despite much larger drop size (peak diameter 28 μm versus 7 μm) and broader size distribution (half width 40 μm versus 2.5 μm), UMTF spray pyrolysis at 120 kHz ultrasonic frequency and 2.3 W electric drive power produced YSZ particles 70% of which were equal to or smaller than those produced using a conventional ultrasonic nebulizer at the much higher frequency of 1.65 MHz and the much higher drive power of 23.5 W.

Moreover, we conclude that in addition to the conventional one particle per drop mechanism [1], spray

pyrolysis may also involve the gas-to-particle conversion mechanism that predicts particles much smaller than the one particle per drop mechanism. Thus, *uniform* nanoparticles can be produced by spray pyrolysis at proper conditions using *uniform* drops of precursor salts with low vapor pressure.

Acknowledgement

Supports by the National Science Foundation, USA under Grant #CTS-98120050, and the National Science Council, Taiwan under Grants #NSC-89-2216-E-01-005 and #NSC-89-2811-E-036-0004, and the Academia Sinica, Taiwan are gratefully acknowledged.

References

1. G. L. MESSING, SHI-CHANG ZHANG and G. V. JAYANTHI, *J. Amer. Ceram. Soc.* **76** (1993) 2707.
2. K. EGUCHI, T. HATAGISHI and H. ARAI, *Solid State Ionics* **86–88** (1996) 1245.
3. S. C. LEE, H. F. LIN, C. Y. TUNG, H. M. LIN and S. L. HSU, *NanoStruct. Mater.* **9** (1997) 697.
4. O. B. MILOSEVIC, M. J. MIRKOVIC and D. P. USKOKOVIC, *J. Amer. Ceram. Soc.* **79** (1996) 1720.
5. S. C. TSAI, P. CHILDS and P. LUU, *AIChE J.* **42** (1996) 3340.
6. S. C. TSAI, P. LUU, P. CHILDS, A. TESHOME and C. S. TSAI, *Phys. of Fluids* **9** (1997) 2909.
7. R. LANG, *J. Acoustic Soc. of Amer.* **34** (1962) 7.
8. S. NUKIYAMA and Y. TANASAWA, *Trans. Jpn. Soc. Mech. Eng.* **5** (1939) 136.
9. S. C. ZHANG and G. L. MESSING, *J. Amer. Ceram. Soc.* **73** (1990) 61.
10. S. C. TSAI, P. LUU, P. TAM, G. ROSKI and C. S. TSAI, *AIP Physics Fluids* **11** (1999) 1331.
11. E. B. SLAMOVICH and F. F. LANGE, *Proc. Mater. Res. Soc.* **121** (1988) 257.
12. T. T. KODAS and M. J. HAMPDEN-SMITH, "Aerosol Processing of Materials" (Wiley-VCH, New York, 1999) Chapts 4, 8 and 11.
13. C. R. BICKMORE, K. F. WALDNER, R. BARANWAL, T. HINKLIN, D. R. TREADWELL and R. M. LAIN, *J. Europ. Ceram. Soc.* **18** (1998) 287.
14. A. SINGHAL, G. SKANDAN, A. WANG, N. GLUMAC, B. H. DEAR and R. D. HUNT, *NanoStruct. Mater.* **11** (1999) 545.
15. K. OKUYAMA, Y. KOUSAKA, N. TOHGE, S. YAMAMOTO, J. J. WU, R. C. FLAGAN and J. H. SEINFELD, *AIChE J.* **32** (1986) 2010.
16. M. ADACHI, K. OKUYAMA, S. MOON, N. TOHGE and Y. KOUSAKA, *J. Mater. Sci.* **24** (1989) 2275.
17. P. P. AHONEN and E. I. KAUPPINEN, *J. Mater. Res.* **14** (1999) 3938.
18. J. H. SEINFELD, "Thermodynamics of Aerosols and Nucleation Theory" (Wiley Interscience, New York, 1986) Chap. 9.
19. G. K. CHUAH, *Catal. Today* **49** (1999) 131.

Received 25 June 2003
and accepted 11 February 2004